Monitoring and adjusting ground-based weather radar in Europe using TRMM space-borne radar

M. Gabella [a,*], J. Joss [b], G. Perona [a], S. Michaelides [c]

[a] Politecnico di Torino, Electronics Department, Corso Duca degli Abruzzi 24, 100129 Torino, Italy – (gabella, perona)@polito.it
[b] Intragna, Switerland – jjo@freesurf.ch; [c] Meteorological Service, Nicosia, Cyprus1601 – silas@avacom.net

Abstract – We show how the TRMM Precipitation Radar (TPR) can be used to monitor and adjust Ground-based Radar (GR) data as a function of the distance from the radar site. The analysis is based on the average, linear radar reflectivity in circular rings around the GR site, $\langle Z \rangle_{2\pi}$, as a function of the range from the GR site. The GR/TPR ratio varies for the Cyprus radar on average from 2 dB, at 10 km, to –10 dB at 100 km. The cause of the average departure at the average range is ascribed mainly to the calibration of the GR. The range dependence of GR/TPR is significant and similar in all the investigated cases. This is attributed to the increasing sampling volume of GR with range combined with non-homogeneous beam filling. For example, at longer ranges of GR, the lower part of the volume could be in rain, whereas the upper part of the same pulse is filled with snow, or even without echo.

Keywords: Space-borne and ground-based meteorological radar. Tropical Rainfall Measuring Mission. Rainfall field.

1. INTRODUCTION

1.1 Earlier studies

Meteorological radar is a good tool to provide a three-dimensional overview of the weather. It shows where and when something is happening in real-time. With the introduction of weather radar onboard the TRMM satellite, used in the Tropical Rainfall Measuring Mission, meteorological radar applications can be extended to a global scale. Ground-based and space-borne sensors provide a complementary view: the Ground-based Radar (GR) measures rain from a lateral direction, whereas the space-borne radar sees it from the top. The differences between the two instruments are large. We recall the different frequency of operation, sampling volume, geometrical viewing angles, attenuation, sensitivity and time of acquisition. Hence, a quantitative comparison between space-borne and ground-based weather radar is a challenge, as shown in several references (e. g., Houze et al., 2004; Amitai et al., 2004). Many efforts have been made to provide the TRMM Precipitation Radar (TPR) with a long-term, continuously monitored electronic stability. The calibration factor is assumed to have accuracy within 1 dB. Consequently TPR provides the possibility of quantitatively assessing the average bias of ground-based radars around the world.

1.2 Concept and overview

We propose a comparison between data from TPR and GR. The concept allows to assess not only the average bias of the GR with respect to the TPR, but also a dependence of the GR-data versus range. TPR allows this assessment, because its measurements originate from similar distances of 400-420 km. GR, on the other hand, measures rain from close to the radar up to large distances from the radar, in our application from 10 to 120 km. Consequently, the scattering volume of GR changes significantly. It increases with the square of the distance from GR, while the change of distance from TPR is small and not correlated with the distance from GR. Therefore, the decrease of sensitivity with range of GR can be estimated using TPR. Sec. 2 briefly describes the geography, instruments and data characteristics of the Mediterranean test site used in this paper. In the literature, the range-dependence of GR-observations has mainly been investigated using in situ rain gauges. In this paper much more data is available than if the analyses would be based on gauges. The comparison between the two instruments is discussed in Sec. 3. Sec. 4 discusses both, results from "simultaneous" GR and TPR echoes, and from daily amounts derived from GR and the Cyprian network of rain gauges. Sec. 5.1 summarizes the advantages and disadvantages of the TRMM-based algorithm compared to conventional range-adjustments based on rain gauge data.

2. THE TEST SITE

2.1 Geography and orography

The island of Cyprus is located in the northeastern corner of the Mediterranean Sea. Therefore, it has a Mediterranean climate: the temperature-rainfall regime is characterized by cool-to-mild wet winters and warm-to-hot dry summers. The island (Fig. 1) is traversed by two mountain ridges, the high Troodos massif in the southwest with the highest peak, Olympus, at ~2000 m above sea level and the long narrow Kyrenia ridge that rises to 900 m, reaching the northern coast. The central plain lies between the two mountain ridges with coastal strips along their seaward sides.
The radar was installed on the northwestern, mountainous region of the island, near Kykkos, a medieval monastery. The radar site, named Kykkos, is at 1310 m above sea level, shown by a white square in Fig. 1. It also illustrates, where data can be recorded using the 0° elevation of GR over Cyprus. The nearby, high Troodos massif causes considerable clutter and behind in the southeast direction, beam shielding. A much narrower sector is shielded to the northwest by the closer Tripylos peak at 1450 m above sea level.

2.2 Ground-based Radar (GR)

Since 1995, the Meteorological Service of Cyprus a C-band Doppler radar, employed in nowcasting applications. Since its installation on the Kykkos site, the radar is used primarily by weather forecasters in issuing warnings for hazardous weather. For this application, the interpretation of the radar products is purely qualitative. But, the radar was modified in 2002 to ease analyses for the VOLTAIRE project. The modifications allow manual storage and archiving of the radar data in digital form, with minimum disturbance, of the operational use of the system by

* Corresponding author: Marco Gabella – gabella@polito.it
This research was co-funded by the European Commission as part of contract EVK2-CT-2002-00155 (VOLTAIRE).

the weather forecasters. Because of the limitations imposed by the lack of manpower, archiving radar data can only be performed for a small number of selected events. Here we analyze rainy events in winter 2002 and 2003. For all days, propagation conditions deduced from the radio-soundings exhibit a quasi-standard decreases in refractivity in the lower atmosphere. Soundings have been launched at 1100 UTC from Nicosia, ~20 km north and 57 km east of the Kykkos radar. The 0ºC isotherm was at ~1900 m on February 11 and 12, 2002 February 3, 2003; on February 4, 2003 it was at ~1600 m. With the antenna at 1325 m above sea level and in standard refractivity conditions, the beam axis reaches a maximum altitude of ~2200 m at the far range.

Fig. 1 shows at 0° elevation the two sectors, where the beam axis hits the mountain ridges. In the GR/TPR comparison no data was used from pixels, either in the shielded sectors or showing any clutter in no-rain situations.

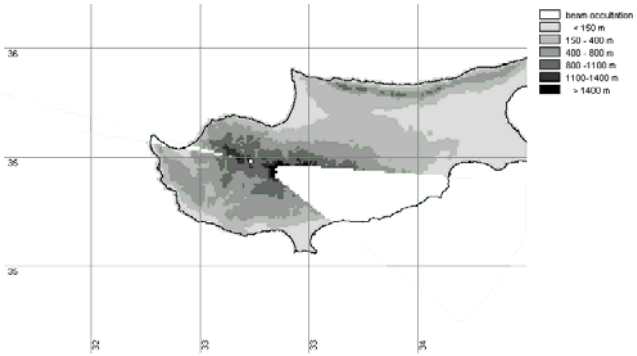

Figure 1. Lat-Lon representation of the orography of Cyprus using 0.01°×0.01° spatial resolution. The 0.5°×0.5° map grid segments are ~55 km along the meridians and ~45 km along the parallels. The white mark shows the Kykkos ground-based radar site almost in the center of the image. The maximum range from the radar is 120 km. Two sectors with considerable beam occultation at 0° elevation are caused by mountains and emphasized using light grey (Troodos, SE direction and Tryplos, NW direction).

2.2 TRMM Precipitation Radar (GR)

A complete description of the Ku-band TRMM Precipitation Radar (TPR) can be found in Kozu et al., 2001. TPR data are attenuation-corrected radar reflectivities obtained at 13.8 GHz with the TRMM 2A25 algorithm, which produces the best estimate of the rain profile. The vertical resolution is 250 m at the nadir. Among the many output variables, available from product 2A25, this study uses the radar reflectivity calculated for the lowest TPR pulse volume, the so-called *NearSurfZ*. Its height is approximately 1.8 km above sea level. For TPR at the scan edge of 18°, light rain is influenced by clutter below ~1.8 km. Below no data is available, because off-nadir, the surface clutter must be eliminated. This limitation depends on the backscattering coefficient of the surface and the rain intensity.

3. RANGE DEPENDENCE OF THE GR AS SEEN BY TPR

3.1 The concept and other efforts

The ground-based radar measures rain from a lateral direction. The distance varies in our case from 10 km to 120 km. Because of this large ratio of distances, the scattering volume changes by a factor of over 100, the volume increasing with the square of the distance. On the other hand, the scattering volume of TPR has similar size in all locations. Furthermore, its size is not correlated from the distance between the echo and the GR. This advantage of TPR stimulated the idea of using TRMM radar to estimate the influence of sampling volume of the ground-based radar.

The divergence of the beam, which is already corrected by the software of the radar, leads to a second phenomenon, which is discussed in the paper. In addition to the $r^{(-2)}$ range dependence, which is corrected in the software, there is the influence of non-homogeneous beam filling. For example, at longer ranges of GR, the lower part of the volume could be in rain, whereas the upper part of the same pulse is filled with snow. This influence becomes larger at longer range, where the pulse volume increases with size.

The difficulties of the dependence from the range of precipitation estimates from ground radars are known for a long time. Together with residual clutter and anomalous propagation these difficulties are the main reason why radars often disappoint meteorologists. It also makes them rarely show precipitation, cumulated over a long time, years: radar-derived images based on large datasets often show circular features around the radar (e. g., Nelson et al., 2003). As mentioned before, these deficiencies are caused not only by decreasing resolution with distance, but also by earth-curvature and beam shielding, combined with non-uniform beam filling.

Deriving a factor for range-correction with distance has often been attempted using rain gauges as a reference: in Nordic countries, the radar-to-gauge ratio was analyzed using multiple regression. It was based on the linear and the square of the distances from the radar as independent variables (e. g., Michelson and Koistinen, 2000). In mountainous regions, the radar/gauge ratio was analyzed using a non-linear weighted multiple regression, based also on the minimum height visible over the gauge and the height of the gauge itself (Gabella et al., 2001). An important influence on the results is caused by the vertical profile of radar reflectivity (VPR) and its variability. The VPR depends on the storm characteristics and its influence on the range adjustment is discussed in many papers. On the other hand, bright band contamination affects both, ground- and spaced-borne systems, in different ways. Here, the derived correction is just a first guess of the needed correction. It proved to be useful in all analyzed overpasses.

3.2 Using a space-borne radar

A space-borne radar gives a complementary view, compared to a ground-based radar. It can give us in a single overpass thousands of remotely sensed estimates over land and sea, much more than land-based *in situ* "point" rain gauge measurements. The addition to conventional radar/gauge-adjustment is the independent variable using data, which are both remotely sensed from space. Furthermore, both, the numerator and denominator of the GR/TPR ratio, are averaged over a rather large area. Gauges on the other hand are local "point" measurements. We compare the ratio of values averaged over many samples at similar range. The range resolution of 10 km is approximately twice the TPR 3 dB beam width. In other words, the volumes used to determine the averages are large, even much larger than the rather coarse TPR-resolution. The large sampling volume reduces mismatches caused by different beam widths and by changes of the weather in space and time. For both radars, we compute the average Z in the same, circular ring. Rings are 10 km wide. Let $\langle GR \rangle_{2\pi}$ and $\langle TPR \rangle_{2\pi}$ be these values of average reflectivity, averaged in azimuth for both the GR and the TPR. Because of their size these two variables show the same behavior, except for the sensitivity of GR. Deviations caused by rain cells of high intensity are reduced by averaging over the large area of the rings. While $< TPR >_{2\pi}$, does not correlate with distance from GR, $\langle GR \rangle_{2\pi}$, tends to decrease

with distance. In this paper, we explain the Factor F = ($<GR>_{2\pi}$)/($<TPR>_{2\pi}$), using a regression between Log(F) and Log(D). To make a_0 reflect the calibration of GR, the predictor D is normalized to D_0, which is a "central" value of D within the analyzed range (10-120 km) of GR (D_0 = 40 km). The slope a_D in Eq.1 reflects the deviation of the radar sensitivity from the common $r^{(-2)}$ law. I.e. it reflects the rate of change of the calibration with distance. We expect and find negative values, since sampling volume of GR increases with the square of the distance, as already mentioned above. It is a consequences of non-homogeneous beam filling, mainly caused by overshooting of precipitation. After trying many types of equations, we found the following to be the best:

$$10 \cdot Log\left(\frac{\langle GR\rangle_{2\pi}}{\langle TPR\rangle_{2\pi}}\right) = F_{dB} = a_0 + a_D \cdot Log\left(\frac{D}{\langle D_0\rangle}\right) \qquad (1)$$

Sec. 4.1 presents results of the regression for a single TRMM overpass. Sec. 4.3 the more robust coefficient, derived by using all available data with couples of four TPR/GR images.

3.3 Projecting TPR-reflectivity on GR-reflectivity

The GR data are acquired using a polar reference system using azimuth and range. The reflectivity of the Cyprus radar bins are sampled with 1 dB resolution, every degree in azimuth and with 500 m resolution in range. Data are stored in a matrix with 360 columns and 240 rows. Each pixel is 1°×500 m. As a consequence, the resolution decreases with distance. The Cartesian range-azimuth display reaches up to 120 km from the radar. This awkward presentation is not area-equivalent. Fig. 2 illustrates this format using the data shown in Fig. 1. Fig. 2 reminds us that the ground-based radar has a larger resolution at a short range than far away.

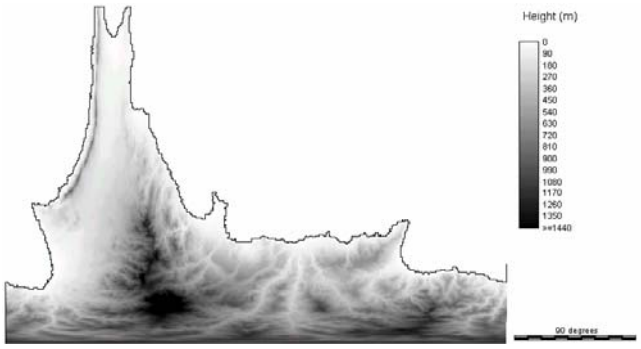

Figure 2. Azimuth-range- (360°-120 km) display of Fig.1 This distorted map was resampled with the resolution of the GR bins (1°×500 m) and is made of 360 columns and 240 rows (range).

Fig. 3 illustrates this format using weather: the top picture was recorded by GR at 00:15 UTC, 13 minutes before the TPR-overpass on February 12, 2002 (center picture). Average values of reflectivity as a function of distance (along circular rings on a PPI), can be derived from these 360×240 images by averaging the linear values of *Z* for each row. In both pictures only valid values are averaged, since we do not want to use reliable TPR-echoes that cannot be seen by the GR because of clutter and shielding.

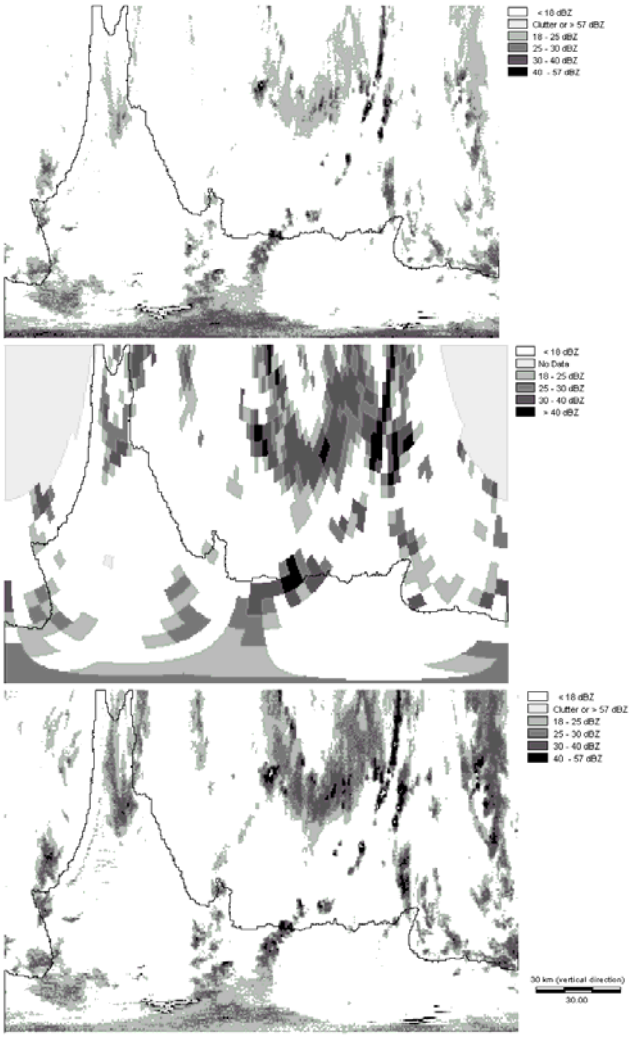

Figure 3. Azimuth-range (360°-120 km) display of the C-band GR (top picture) and Ku-band space-borne TPR (center picture). GR data were acquired at 00:15, the TPR data at 00:28 UTC. TPR data have been resampled onto the GR polar reference system (radar bins of 1°×500 m). As in Fig. 2, the image is 360×240. Range-adjusted GR echoes are plotted in the bottom picture.

4. RESULTS

4.1 Bias and range dependence from a single overpass

The overpass with the largest "rainy" area was recorded on February 12: as shown in Table 1, in an area of 5850 km^2 the TPR reflectivity was larger than 25 dBZ. For this overpass, the regression gives best results for a single TRMM overpass with an explained variance of 60%. The adjustment coefficients are:

$$F_{dB} = -4.4 - 12.9 \cdot Log\left(D/\langle D_0\rangle\right) \qquad (2)$$

The range of validity of *D* is between 10 and 120km. The central value D_0 was set to 40 km. The explained variance is smaller for the other three overpasses. However, the values of a_0 and a_D are relatively "stable" for all single overpasses and also for the sum of all overpasses. Both, a_0 and a_D are always negative. In short, we find at 10 km a few dB overestimation, while at 120 km Eq. (2)

gives a large underestimation. We should not emphasize the overestimation at short ranges, because many difficult guesses had to be made for solving the radar equation. As mentioned in Sec. 1.2, TPR echoes have no reason to depend on the distance from the GR site. Hence, if the GR/TPR ratio always decreases with distance, at least a first order correction should be feasible. By adjusting the GR reflectivity using Eq. (2), the bottom picture in Fig. 3 is obtained. Comparing the bottom image (range-adjusted) and the original one (top picture), with TPR in the center, show a positive influence of the correction. An evaluation of the improvement is given in the next Sec. 4.2, where rainy areas of GR and of TPR are compared. In Sec. 4.3, the results are based on the more robust values of a_0 and $a_{D,}$ Eq.(3) instead of Eq. (2). These more robust values are presented and discussed there.

4.2 Comparing rainy area before and after range-adjustment

Table 3 gives the influence of the range-adjustment on the size of the rainy area in single TPR overpasses. The area with reflectivity above a threshold increases significantly after correction. This is true for any reflectivity threshold. Table 3 summarizes the results for a threshold of 25 dBZ. This threshold is well above the TPR noise and attenuation does not yet influence propagation significantly. Let us continue our analysis from the overpass presented in the previous section (February 12, 2002). The range-adjustment causes, on average, a remarkable increase of the area for echoes larger than 25 dBZ.

The same happens for the previous TRMM overpass (22:50 UTC on February 11) The sensitivity of the GR decreases with range. This results in an overall underestimation, which was also observed in winter 2003, e. g., on February 3 and 4.

Table 1. Total and percentage area with radar reflectivity over 25 dBZ. The decrease of sensitivity with range of the GR, results in a general underestimation. After the range-adjustment, better agreement of the rainy area is obtained. Similar percentage ratios were observed for thresholds of 20 and 30 dBZ

Date	Radar data type	Area ≥25 dBZ	% of area with respect to TPR
Feb. 11, 2002	GR *raw data*	*1695* km^2	*41%*
	GR **range-adjusted**	**3192** km^2	**78%**
	TPR "NearSurfZ"	4100 km^2	100%
Feb. 12, 2002	GR *raw data*	*1463* km^2	*25%*
	GR **range-adjusted**	**5245** km^2	**89%**
	TPR "NearSurfZ"	5850 km^2	100%
Feb. 3, 2003	GR *raw data*	*147* km^2	*37%*
	GR **range-adjusted**	**260** km^2	**65%**
	TPR "NearSurfZ"	400 km^2	100%
Feb. 4, 2003	GR *raw data*	*886* km^2	*30%*
	GR **range-adjusted**	**3286** km^2	**111%**
	TPR "NearSurfZ"	**295**0 km^2	100%

4.1 A robust correction: using all overpass

As described above, small samples may lead to errors, e. g., of single overpasses. To increase the sample size, all available overpasses are integrated. The resulting correction parameters are shown in the last line of Table 2. The dependence of the factor on the distance is depicted in Fig. 6. The variance explained increases from 0.6 for the best, single overpass to 0.8 for the regression using the data of all four overpasses added together (Eq.3).

$$F_{dB} = -3.5 - 11.8 \cdot Log\left(D/\langle D_0 \rangle\right) \qquad (3)$$

The explained variance raises to 80%: we conclude that the summation of the data of four overpasses helps to reduce the uncertainties of the offset a_0 and the slope a_D. The part remaining of the variability of the GR/TPR ratio, which is not explained by the regression coefficients, is caused by the weather situation with the variability of the VPR, including the bright band.

5. SUMMARY

When and where available, the space-borne radar can be used to monitor and adjust meteorological Ground-based Radars (GR). The GR scattering volume increases with the square of the distance, while it is almost constant for space-borne radar. This paper shows how space-borne radar can be used to adjust GR estimates. The correction is obtained by calculating the "azimuth-integral" of the radar reflectivity at constant range. In this way, the range dependence of both radars along the radial direction can be compared. Their ratio, on a logarithmic scale versus the Distance, also on a logarithmic scale, is statistically analyzed. As a result, the adjustment factor versus distance is found. The underestimation of ground-based radars at far ranges has often been verified in literature by using rain gauges [18]-[20]. It has been verified using time-cumulated rain gauge amounts. Here, we use a space-borne radar, which permits more robust results to be obtained because of three reasons: (1) the larger number of samples being averaged at similar ranges; (2) the volumetric nature of these samples, instead of gauge "point" measurements; (3) the possibility of covering land and sea, where no gauges are available.

6. REFERENCES

R. A. Houze, S. Brodzik, C. Schumacher, and S. E. Yuter, "Uncertainties in oceanic radar maps at Kwajalein and imlications for satellite validation," *J. Appl. Meteorol.*, vol. 43, pp. 1114-1132, 2004.

E. Amitai, J. A. Nystuen, L. Liao, R. Meneghini, E. Morin, "Uniting space, ground, and underwater measurements for improved estimates of rain rate". *IEEE Geosci. Remote Sensing Letters*, vol. 1, pp. 35-38, 2004.

T. Kozu, T. Kawanishi, H. Kuroiwa, M. Kojima, K. Oikawa, H. Kumagai, K. Okamoto, M. Okumura, H. Nakatsuka, and K. Nishikawa, "Development of Precipitation Radar Onboard the Tropical Rainfall Measuring Mission (TRMM) Satellite". *IEEE Trans. Geosci. Remote Sensing*, vol. 39, pp.102–115, 2001.

B.R. Nelson, W.F. Krajewski, A. Kruger, J.A. Smith, M.L. Baeck, "Archival precipitation data set for the Mississippi River Basin: Algorithm development". *J. Geophys. Res.*, vol. 108(D22), doi:10.1029/2002JD003158, 8857, 2003.

D. B. Michelson, J. Koistinen, "Gauge-radar network adjustment for the Baltic Sea experiment". *Phys. Chem. Earth (B)*, vol. 25, pp. 915–920, 2000.

M. Gabella, J. Joss, and G. Perona, "Optimizing quantitative precipitation estimates using a non-coherent and a coherent radar operating on the same area". *J. Geophys. Res.*, vol. 105, pp. 2237-2245, 2000.